Switching energy limits of waveguide-coupled graphene-on-graphene optical modulators

Steven J. Koester,* Huan Li, and Mo Li

Dept. of Electrical & Computer Engineering, University of Minnesota-Twin Cities, Minneapolis, MN 55455, USA
skoester@umn.edu

Abstract: The fundamental switching energy limitations for waveguide coupled graphene-on-graphene optical modulators are described. The minimum energy is calculated under the constraints of fixed insertion loss and extinction ratio. Analytical relations for the switching energy both for realistic structures and in the quantum capacitance limit are derived and compared with numerical simulations. The results show that sub-femtojoule per bit switching energies and peak-to-peak voltages less than 0.1 V are achievable in graphene-on-graphene optical modulators using the constraint of 3 dB extinction ratio and 3 dB insertion loss. The quantum-capacitance limited switching energy for a single TE-mode modulator geometry is found to be < 0.5 fJ/bit at λ = 1.55 μm, and the dependences of the minimum energy on the waveguide geometry, wavelength, and graphene location are investigated. The low switching energy is a result of the very strong optical absorption in graphene, and the extremely-small operating voltages needed as the device approaches the quantum capacitance regime.

OCIS codes: (250.4110) Modulators; (250.7360) Waveguide modulators.

References and links

1. F. Xia, T. Mueller, Y. M. Lin, A. Valdes-Garcia, and P. Avouris, "Ultrafast graphene photodetector," Nat. Nanotechnol. **4**(12), 839–843 (2009).
2. T. Mueller, F. Xia, and P. Avouris, "Graphene photodetectors for high-speed optical communications," Nat. Photonics **4**(5), 297–301 (2010).
3. M. Liu, X. Yin, E. Ulin-Avila, B. Geng, T. Zentgraf, L. Ju, F. Wang, and X. Zhang, "A graphene-based broadband optical modulator," Nature **474**(7349), 64–67 (2011).
4. B. Sensale-Rodriguez, R. Yan, M. M. Kelly, T. Fang, K. Tahy, W. S. Hwang, D. Jena, L. Liu, and H. G. Xing, "Broadband graphene terahertz modulators enabled by intraband transitions," Nat. Commun. **3**, 780 (2012).
5. Q. Bao, H. Zhang, B. Wang, Z. Ni, C. H. Y. X. Lim, Y. Wang, D. Y. Tang, and K. P. Loh, "Broadband graphene polarizer," Nat. Photonics **5**(7), 411–415 (2011).
6. Z. Sun, T. Hasan, F. Torrisi, D. Popa, G. Privitera, F. Wang, F. Bonaccorso, D. M. Basko, and A. C. Ferrari, "Graphene mode-locked ultrafast laser," ACS Nano **4**(2), 803–810 (2010).
7. Q. Bao, H. Zhang, Y. Wang, Z. Ni, Y. Yan, Z. X. Shen, K. P. Loh, and D. Y. Tang, "Atomic-layer graphene as a saturable absorber for ultrafast pulsed lasers," Adv. Funct. Mater. **19**(19), 3077–3083 (2009).
8. X. Li, W. Cai, J. An, S. Kim, J. Nah, D. Yang, R. Piner, A. Velamakanni, I. Jung, E. Tutuc, S. K. Banerjee, L. Colombo, and R. S. Ruoff, "Large-area synthesis of high-quality and uniform graphene films on copper foils," Science **324**(5932), 1312–1314 (2009).
9. B. Jalali and S. Fathpour, "Silicon photonics," IEEE J. Lightwave Tech. **24**(12), 4600–4615 (2006).
10. S. J. Koester and M. Li, "High-speed waveguide-coupled graphene-on-graphene optical modulators," Appl. Phys. Lett. **100**(17), 171107 (2012).
11. M. Liu, X. Yin, and X. Zhang, "Double-layer graphene optical modulator," Nano Lett. **12**(3), 1482–1485 (2012).
12. D. A. B. Miller, "Energy consumption in optical modulators for interconnects," Opt. Express **20**(S2 Suppl 2), A293–A308 (2012).
13. F. Y. Gardes, D. J. Thomson, N. G. Emerson, and G. T. Reed, "40 Gb/s silicon photonics modulator for TE and TM polarisations," Opt. Express **19**(12), 11804–11814 (2011).
14. T. Fang, A. Konar, H. Xing, and D. Jena, "Carrier statistics and quantum capacitance of graphene sheets and ribbons," Appl. Phys. Lett. **91**(9), 092109 (2007).
15. Z. Q. Li, E. A. Henriksen, Z. Jiang, Z. Hao, M. C. Martin, P. Kim, H. L. Stormer, and D. N. Basov, "Dirac charge dynamics in graphene by infrared spectroscopy," Nat. Phys. **4**(7), 532–535 (2008).
16. J. Horng, C.-F. Chen, B. Geng, C. Girit, Y. Zhang, Z. Hao, H. A. Bechtel, M. Martin, A. Zettl, M. F. Crommie, Y. R. Shen, and F. Wang, "Drude conductivity of Dirac fermions in graphene," Phys. Rev. B **83**(16), 165113 (2011).

#169845 - $15.00 USD Received 13 Jun 2012; revised 11 Aug 2012; accepted 11 Aug 2012; published 20 Aug 2012

17. G. W. Hanson, "Dyadic Green's functions and guided surface waves for a surface conductivity model of graphene," J. Appl. Phys. **103**(6), 064302 (2008).
18. J. D. Joannopoulos, *Photonic Crystals: Molding the Flow of Light, 2nd edition* (Princeton University Press, 2008).
19. H. Li, Y. Anugrah, S. J. Koester, and M. Li, "Optical absorption in graphene integrated on silicon waveguides," arXiv:1205.4050v1, 2012.
20. M. R. Watts, W. A. Zortman, D. C. Trotter, R. W. Young, and A. L. Lentine, "Vertical junction silicon microdisk modulators and switches," Opt. Express **19**(22), 21989–22003 (2011).
21. J. Liu, M. Beals, A. Pomerene, S. Bernardis, R. Sun, J. Cheng, L. C. Kimerling, and J. Michel, "Waveguide-integrated, ultralow-energy GeSi electro-absorption modulators," Nat. Photonics **2**(7), 433–437 (2008).
22. N.-N. Feng, D. Feng, S. Liao, X. Wang, P. Dong, H. Liang, C.-C. Kung, W. Qian, J. Fong, R. Shafiiha, Y. Luo, J. Cunningham, A. V. Krishnamoorthy, and M. Asghari, "30GHz Ge electro-absorption modulator integrated with 3 μm silicon-on-insulator waveguide," Opt. Express **19**(8), 7062–7067 (2011).
23. R. K. Schaevitz, E. H. Edwards, J. E. Roth, E. T. Fei, Y. Rong, P. Wahl, T. I. Kamins, J. S. Harris, and D. A. B. Miller, "Simple electroabsorption calculator for designing 1310 nm and 1550 nm modulators using germanium quantum wells," IEEE J. Quantum Electron. **48**(2), 187–197 (2012).
24. S. Ren, Y. Rong, S. A. Claussen, R. K. Schaevitz, T. I. Kamins, J. S. Harris, and D. A. B. Miller, "Ge/SiGe quantum well waveguide modulator monolithically integrated with SOI waveguides," IEEE Photon. Technol. Lett. **24**(6), 461–463 (2012).

1. Introduction

Graphene is a promising material for optoelectronic applications, due to its relatively high absorption coefficient, broad spectral range of absorption, and excellent transport properties. Recently, numerous demonstrations of graphene optoelectronic devices have been made, including photodetectors [1,2], modulators [3,4] polarization controllers [5] and ultra-fast pulsed lasers [6,7]. Furthermore, the ability to produce wafer-scale, single-layer graphene with good material quality [8] and transfer it onto Si substrates makes practical application of graphene for optoelectronic devices a strong near-term possibility. Graphene integrated with silicon photonics is especially interesting, since Si photonics can provide an outstanding platform for integration with CMOS circuits [9]. However, in assessing whether or not such devices would be of use for optical communications applications, the energy consumption must be determined and compared with alternative geometries.

As a starting point, a particularly interesting device to investigate is the graphene-on-graphene optical modulator described both theoretically [10] and experimentally [11]. Such a device lends itself well to theoretical treatment due to its simple parallel plate geometry, and the fact that under ideal circumstances, no DC current flows in the device. Therefore, its total energy consumption can be analyzed using a similar analysis to other types of optical modulators that can be integrated with silicon photonics [12]. In this paper, the fundamental energy limits of graphene-on-graphene optical modulators are analyzed. First, the device geometry and general assumptions are described. Then an analytical treatment for the device operation is provided, leading to an open form expression of the fundamental limit of the switching energy. Subsequently, numerical simulations are used to optimize design parameters of different device configurations and to reach the practical switching energy limit. Finally, a discussion of the implications and restrictions of this analysis is provided.

2. Modulator structure

The basic graphene-on-graphene optical modulator structure has been described previously [10] and is shown schematically in Fig. 1. The nominal device structure consists of two graphene layers separated by a thin dielectric, located on a photonic waveguide. In these calculations, Si was used as the waveguide core, and was surrounded on all sides by SiO_2 cladding layers. The graphene dual-layer structure is placed either in the center or on top of the waveguide core. For the calculations below, we have made the simplifying assumption that the graphene does not perturb the optical mode, and that the distance between the two graphene layers is sufficiently small compared to the size of the optical mode so that the two layers have the same absorption properties. Using numerical simulations, we have found this to be a reasonable assumption for graphene interlayer spacing of less than ~10 nm. We have further assumed that the graphene width is simply the width of the waveguide core, and that

#169845 - $15.00 USD Received 13 Jun 2012; revised 11 Aug 2012; accepted 11 Aug 2012; published 20 Aug 2012

the connecting leads to the graphene (not shown in the figure) do not contribute to optical absorption. This assumption is justified since absorption in the leads could be suppressed by heavily doping the graphene in these regions, and/or by limiting the leads to specific locations along the length of the modulator. As shown in Fig. 1, the calculations further assume that the device has been tuned to operate at the ideal operating conditions for maximum extinction ratio, where both graphene layers are utilized as gate-tunable absorbers [10]. In particular, this condition occurs when $E_{F(\text{top})} = -hc/2\lambda$ and $E_{F(\text{bottom})} = +hc/2\lambda$, where $E_{F(\text{top})}$ and $E_{F(\text{bottom})}$ are the Fermi energies relative to the Dirac point in the top and bottom layers respectively, h is Planck's constant and λ is the wavelength. Such a situation could be achieved either by applying a DC bias between the layers, or by precisely doping the top and bottom graphene to be p- and n-type respectively. While the former approach might be less challenging to fabricate, the latter would allow the modulator to operate at zero DC bias, thus ensuring that no DC power is consumed in the biasing electronics. We also assume that the Si waveguide is undoped and that the bias voltages applied to the graphene layers do not induce charges in the Si so that no additional free carrier absorption is caused. Finally, we assume that no leakage current flows between the graphene sheets.

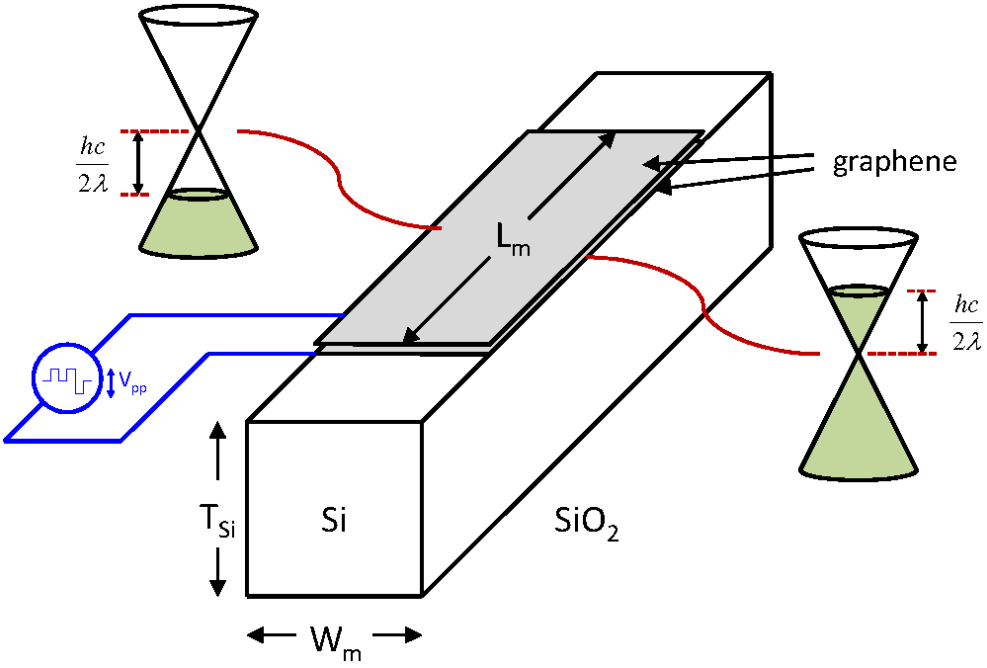

Fig. 1. Schematic diagram of graphene-on-graphene modulator. The device consists of a Si waveguide core with SiO_2 cladding on all sides. A voltage is applied between the graphene sheets which modulates the Fermi-level in both layers. In this work, it is assumed that at zero bias, the Fermi-level positions in the two graphene sheets are at $\pm hc/2\lambda$. The graphene sheets are assumed to be separated by a thin dielectric layer and can be positioned either at the top of the waveguide core (as shown above) or embedded within the center of the waveguide core.

3. Energy calculation

Based upon the above structural assumptions, the minimum energy can be calculated as follows. First, it is assumed that a non-return-to-zero (NRZ) data transmission scheme [13] is utilized so the energy dissipation, E, of the modulator can be expressed as:

$$E = \frac{1}{4} C_m V_{pp}^2, \qquad (1)$$

#169845 - $15.00 USD Received 13 Jun 2012; revised 11 Aug 2012; accepted 11 Aug 2012; published 20 Aug 2012

where C_m and V_{pp} are the modulator capacitance and peak-to-peak voltage, respectively. The ¼ term in (1) comes from the fact that in an NRZ signaling scheme, and for a random bit sequence, one complete charge/discharge cycle occurs on average once every four bits.

The value of C_m for the modulator can then be calculated as

$$C_m = \frac{0.5 c_{ox} c_Q}{c_{ox} + 0.5 c_Q} \cdot (W_m L_m), \tag{2}$$

where c_{ox} is the oxide capacitance per unit area associated with the dielectric separating the two graphene layers, c_Q is the quantum capacitance (per unit area) in each graphene sheet, W_m is the modulator width and L_m is the modulator length. Once again, in (2), it is assumed that the modulator is operated in the regime that provides maximum extinction ratio, which occurs when the Fermi levels in the top and bottom layers are $\pm hc/2\lambda$ from the Dirac point energy. In this condition, and in the limit of small spacing between the graphene sheets, both graphene layers contribute equally to optical modulation. The potential movement, ΔV, in each graphene layer required to achieve a specified degree of modulation will be proportional to the thermal energy and can be expressed as

$$\Delta V = 2m \frac{kT}{e}, \tag{3}$$

where k is Boltzmann's constant, T is temperature, e is the electronic charge, and m is a term we call the "modulation coefficient." This potential change will need to appear across both graphene layers, and therefore, the minimum peak-to-peak applied voltage needed to achieve a specific degree of modulation can be expressed as

$$V_{pp} = 2\Delta V + V_{ox} = 4m \frac{kT}{e} \cdot \left(1 + \frac{c_Q}{2c_{ox}}\right), \tag{4}$$

where V_{ox} is the voltage dropped across the oxide separating the graphene layers. The quantum capacitance per unit area, c_Q, in single-layer graphene [14] can be expressed as

$$c_Q = \frac{8e^2 \pi kT}{h^2 v_F^2} \cdot \ln\left[2\left(1 + \cosh\left(\frac{hc}{2kT\lambda}\right)\right)\right], \tag{5}$$

where e is the electronic charge, h is Planck's constant, v_F is the Fermi velocity, and λ is the wavelength. The quantum capacitance relation can be greatly simplified for photon energies much larger than the thermal energy. In this case, the quantum capacitance reduces to

$$c_Q \approx \frac{4\pi e^2 c}{h v_F^2 \lambda}. \tag{6}$$

The oxide capacitance per unit area can be expressed using the standard parallel-plate formula

$$c_{ox} = \frac{3.9\varepsilon_0}{EOT}, \tag{7}$$

where 3.9 is the relative dielectric constant of SiO_2, ε_0 is the permittivity of free space and EOT is the equivalent oxide thickness of the dielectric separating the graphene layers. This is an excellent assumption when $EOT << W_m, L_m$, which is likely to be valid for most practical designs.

It is convenient to express L_m in terms of the absorption coefficient, α_0, so we can write:

#169845 - $15.00 USD Received 13 Jun 2012; revised 11 Aug 2012; accepted 11 Aug 2012; published 20 Aug 2012

$$L_m = \frac{\gamma}{\alpha_0}, \tag{8}$$

where γ is a dimensionless proportionality coefficient. Now, in order to determine the performance parameters of the device, we first define an expression for the modulator loss, *L*. Here, we define the loss (in dB) as:

$$L = -10\log(T_{\max}). \tag{9}$$

where $T_{\max}$, is the maximum transmission coefficient within a modulator cycle. $T_{\max}$, can then be expressed as:

$$T_{\max} = \exp\left(-\frac{2\gamma}{1+e^m}\right). \tag{10}$$

In (10), the main exponential accounts for the decaying optical intensity along the length of the modulator. The factor of two inside the exponential represents the fact that both top and bottom graphene layers are contributing to absorption. Finally, the $1/(1 + e^m)$ term is simply the Fermi-Dirac occupation probability when E_F is at its furthest distance from the Dirac point (i.e., when $E_F = \pm (hc/2\lambda + mkT)$). It should be pointed out that (10) only accounts for optical modulation associated with Pauli blocking [15] of inter-band transitions and ignores the free-carrier (intra-band) contribution to the optical absorption [16]. This is a reasonable assumption given the fact that the voltage is only modulated around $E_F = \pm hc/2\lambda$ by a few *kT*, and optical absorption due to intra-band transitions is small compared to the residual inter-band absorption. Such effects may have to be taken into account if much larger extinction ratios, very low insertion loss or very long wavelength operation are desired.

In a similar manner to the insertion loss, the extinction ratio, *ER*, can be expressed (in dB) as the ratio of the maximum to minimum transmission coefficients, $T_{\max}$ and $T_{\min}$, respectively, during a full gate modulation cycle:

$$ER = 10\log(T_{\max}/T_{\min}), \tag{11}$$

where $T_{\max}/T_{\min}$ can be expressed as

$$T_{\max}/T_{\min} = e^{2\gamma\beta}, \tag{12}$$

and β is related to the modulation coefficient, *m*, by:

$$\beta = \frac{e^m - 1}{e^m + 1}. \tag{13}$$

Equations (8)-(13) can be solved to determine γ and *m* for specific values of *L* and *ER*. Here, we assume values of *ER* = 3 dB and *L* = 3 dB, and solve to obtain:

$$\gamma = \frac{3}{2}\ln(2), \tag{14}$$

and

$$m = \ln(2). \tag{15}$$

From Eqs. (4) and (7), it can be seen that the switching voltage decreases as the *EOT* is reduced. In a normal parallel plate capacitor, c_{ox} would increase inversely proportional to *EOT*, but in a graphene-on-graphene structure, the capacitance increase is limited by the quantum capacitance, and reaches a maximum finite value as c_{ox} approaches infinity. In this so-called quantum capacitance limit, the minimum voltage and the associated capacitance values can be expressed as:

#169845 - $15.00 USD Received 13 Jun 2012; revised 11 Aug 2012; accepted 11 Aug 2012; published 20 Aug 2012

$$V_{pp} = 4 \cdot \ln(2) \cdot \frac{kT}{e}, \tag{16}$$

and

$$C_m = \frac{c_Q}{2} \cdot W_m \cdot \frac{3\ln(2)}{2\alpha_0}. \tag{17}$$

Combining Eqs. (6) and (17), the zero-thickness capacitance can be expressed as:

$$C_m = \frac{3\pi e^2 c}{h v_F^2 \lambda} \cdot W_m \cdot \frac{\ln(2)}{\alpha_0}. \tag{18}$$

Inserting Eqs. (16) and (18) into (1), and utilizing the relation that $(\ln(2))^3 \approx 1/3$, we obtain for the switching energy:

$$E \approx \frac{4c}{v_F^2} \cdot \left(\frac{kT}{e}\right)^2 \cdot \frac{\pi e^2}{h\alpha_0} \cdot \frac{W_m}{\lambda}. \tag{19}$$

Finally, to see how this switching energy is related to the operation wavelength, we assume that the waveguide cross-sectional dimensions, T_{Si} and W_m both scale proportionally to λ. Then the strength of the electric field in the plane of the graphene is reduced by a factor of λ^2 if the optical power is kept constant. However, since we assume that the graphene sheet width is equal to W_m, then it follows that the linear absorption coefficient, α_0, will scale as $1/\lambda$. Given these assumptions, and expressing α_0 in terms of the universal optical absorption, we obtain:

$$E \approx 8 \cdot \frac{c\lambda}{v_F^2} \cdot \left(\frac{kT}{e}\right)^2 \cdot \frac{w}{a}, \tag{20}$$

where

$$\alpha_0 = \frac{a}{\lambda} \cdot \frac{\pi e^2}{2h}, \tag{21}$$

and

$$W_m = w\,\lambda. \tag{22}$$

Inserting the values $T = 300$ K and $v_F = 1.1 \times 10^6$ m/s, then Eq. (20) simplifies to:

$$E \approx 1.33 \times 10^3 \cdot \lambda \cdot \left(\frac{w}{a}\right) \text{fJ}, \tag{23}$$

where λ is in units of μm, a is in units of Ω and w is dimensionless. Thus, under the criteria defined above, the switching energy at a given wavelength is solely determined by the values of a and w. It also follows that the wavelength-dependent minimum switching energy, $E_{\min}$, occurs when the minimum value of the ratio, w/a, for a given graphene/waveguide configuration, is reached. In the following section, we present the results of our $E_{\min}$ calculations for several different device geometries.

4. Calculation and optimization results

In this work, we have focused on the design of practical devices that have low switching energy and can be readily fabricated, rather than searching for the ultimate minimal switching energy that can only be achieved with an impractical device. Graphene/waveguide

#169845 - $15.00 USD Received 13 Jun 2012; revised 11 Aug 2012; accepted 11 Aug 2012; published 20 Aug 2012

configurations which consist of a rectangular Si core surrounded by SiO_2 cladding have been considered, and the switching energy of various device configurations have been calculated to determine the optimal modulator structure that provides the lowest value of *w/a*. For simplicity, we have focused on waveguide structures supporting only the fundamental TE and TM modes, since multimode operation is generally undesirable in optical modulators. Three particular waveguide geometries with the graphene-on-graphene layers residing either in the middle or on the top of the Si waveguide core have been simulated.

For these simulations, the optical properties of the graphene were calculated as follows. The graphene was modeled as an infinitely thin conducting sheet which has only in-plane conductivity and only interacts only with the tangential (in-plane) component of the electric field, E_t. The complex 2D conductivity was calculated from the Kubo formula [17] using Fermi-level and wavelength values representative of the operating conditions described in the previous section. For example, when $E_F = hc/2\lambda + kT\ln(2)$, and assuming a scattering energy of $\hbar\Gamma = 5\text{meV}$, T = 300 K, and λ = 1.55 μm, the calculated conductivities are: $\sigma_{\text{intra}} = (0.505 - 40.5i)\ \mu\text{S}$, $\sigma_{\text{inter}} = (21.3 + 64.9i)\ \mu\text{S}$, and $\sigma_{\text{tot}} = (21.8 + 24.5i)\ \mu\text{S}$. Here, σ_{intra} and σ_{inter} are the complex optical conductivities associated with intra-band and inter-band absorption, respectively, and $\sigma_{tot} = \sigma_{intra} + \sigma_{inter}$ is the total optical conductivity. As stated previously, because the real part of the intra-band conductivity is much smaller than the inter-band portion, intra-band absorption was ignored in the energy calculations in section 3.

We incorporated graphene with the above optical properties into an optical finite element method (FEM) simulator using the following boundary condition between the dielectric materials on both sides of the graphene and solved for the electric field:

$$\mathbf{n}\times(\mathbf{H}_1 - \mathbf{H}_2) = \sigma\left[\mathbf{n}\times(\mathbf{E}\times\mathbf{n})\right]. \tag{24}$$

Here **n** is the unit vector normal to the graphene layer, $\mathbf{H}_1$ and $\mathbf{H}_2$ are the magnetic fields on both sides of the graphene layer, σ is the complex conductivity and **E** is the electric field at the graphene layer.

The structures and calculated mode profiles for the three waveguide geometries are shown below in Fig. 2. In this figure, the square of the in-plane component of electric field, $|E_t|^2$, is plotted vs. position in the waveguide. Each structure was analyzed to obtain the values of *w/a* that are needed to determine the minimum switching energy of the modulator. The simulation suggests that in all of the cases considered here, the presence of the graphene layers has a negligible perturbation to the optical mode, so that the optical absorption is proportional to the real portion of the graphene conductivity. We have also neglected material dispersion, which is a valid approximation for Si and SiO_2 in the considered wavelength range (λ = 1.55 – 3.5 μm).

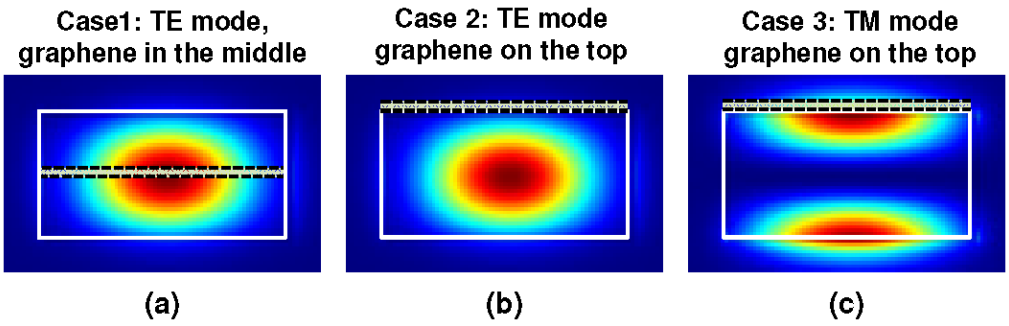

Fig. 2. Simulation results showing mode profiles of the in-plane electric field magnitude, $|E_t|^2$, for three different graphene/waveguide structures. Graphene-on-graphene located (a) in the middle of the core of a fundamental TE mode waveguide, (b) on top of the core of a fundamental TE mode waveguide, and (c) on top of the core of a fundamental TM mode waveguide.

#169845 - $15.00 USD Received 13 Jun 2012; revised 11 Aug 2012; accepted 11 Aug 2012; published 20 Aug 2012

The FEM simulations described above were used to calculate the graphene absorption for different waveguide dimensions (thickness and width) at various wavelengths. We systematically investigated the three different situations shown above, and examined the parameters that provide the lowest switching energy. It can be shown that the waveguide structure (including graphene) and the optical mode scale linearly with the wavelength whereas the graphene absorption coefficient scales inversely with the wavelength, justifying Eq. (21). These scaling properties can be deduced from the fundamental scaling laws of the optical mode [18], with the consideration that the presence of the two-dimensional graphene induces a negligible perturbation to the optical mode. The wavelength scaling properties allow us to present the results using parameters normalized to wavelength. In Fig. 3, the simulation results are shown, where the switching energy E is plotted vs. the normalized waveguide width w for several values of the normalized waveguide thicknesses, $t = T_{Si}/\lambda$, under the requirement that the waveguide supports the fundamental TE and TM modes. For each configuration, and for a given value of t, the energy has a minimum at a specific value of w, and for a particular value of t, a global minimum energy value, E_{min}, is reached.

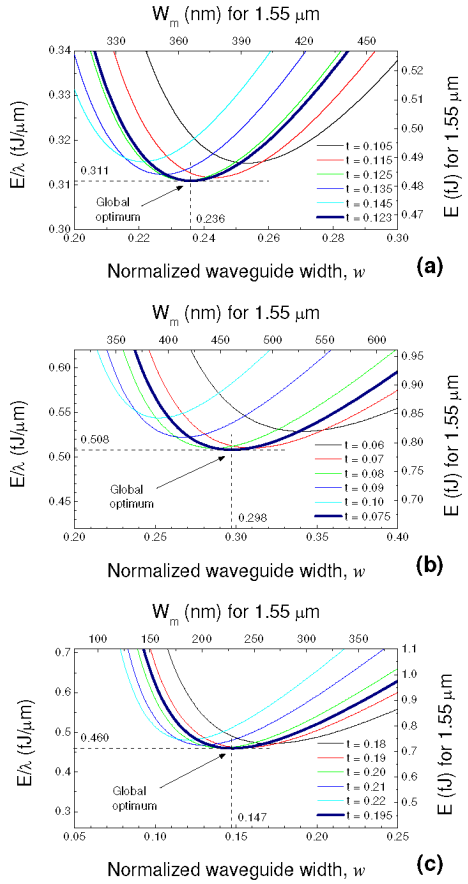

Fig. 3. Plot of global waveguide optimization for waveguide geometries shown in Fig. 2. The optimization is shown for graphene-on-graphene located (a) in the middle of the core of a fundamental TE mode waveguide, (b) on top of the core of a fundamental TE mode waveguide, and (c) on top of the core of a fundamental TM mode waveguide. In all of the plots, the switching energy normalized to wavelength, E/λ, is plotted on the left axis vs. the normalized width, w, for several values of normalized waveguide thickness, t. In each of the graphs, the absolute value of E can be calculated by multiplying the normalized value on the left axis by λ. On the right axis, E has been plotted for λ = 1.55 μm. In each case, the minimum switching energy, E_{min}, can be determined from the global optimum point, which occurs for specific values of w and t. In all cases, $ER = L = 3$ dB.

#169845 - $15.00 USD Received 13 Jun 2012; revised 11 Aug 2012; accepted 11 Aug 2012; published 20 Aug 2012

A summary of the modulator design optimization results are shown in Table I, where the dimensions and the corresponding minimum switching energies are listed, for both λ = 1.55 μm and λ = 3.5 μm. The wavelength dependence of E_{min} for the three different modulator designs is also shown in Fig. 4(a), confirming the wavelength scaling property. A minimum switching energy of 0.48 fJ/bit occurs for Case 1 (the TE-mode / embedded graphene design) at λ = 1.55 μm, a value that increases to 1.09 fJ/bit at λ = 3.5 μm. Comparing the two TE configurations, placing the graphene layers in the middle (Case 1) instead of on the top surface (Case 2) of the waveguide core reduces the optimal switching energy by 40%. This improvement is due to the much higher in-plane electric field in the middle of the Si core compared to on the top surface. The minimum energy associated with the TM mode when the graphene layers are on the top surface (Case 3) is comparable to that for the TE mode (Case 2). Although the linear absorption coefficient for the TE mode is higher than for the TM mode, the TE mode design requires a wider waveguide, and thus leads to an increased device capacitance. Conversely, the TM-mode design allows the waveguide to be narrower, making up for the lower absorption. In addition, we point out that the absorption coefficients calculated from the simulation results in Fig. 3 for the TE-mode / graphene-on-top structure are in excellent agreement with our experimental results for graphene-on-waveguide structures [19].

In Fig. 4(b), E_{min} is also plotted vs. *ER* at λ = 1.55 μm for the three waveguide configurations. It can be seen that as *ER* increases, E_{min} also increases due to the much higher AC voltage needed to shift the Fermi level over a greater energy range in the graphene. As a reminder, free carrier absorption was not included in these calculations, and while this is reasonable assumption at λ = 1.55 μm, at longer wavelengths, free carrier absorption could become a factor and limit the achievable extinction ratios.

Table I. Optimized waveguide parameters used in minimum energy calculations.

Case #	Optimal $w = W_m/\lambda$	Optimal $t = T_{Si}/\lambda$	Minimum Switching Energy E_{min}		
			Normalized (fJ/μm)	1.55 μm (fJ)	3.5 μm (fJ)
1	0.236	0.123	0.311	0.482	1.09
2	0.298	0.075	0.508	0.788	1.78
3	0.147	0.195	0.460	0.713	1.61

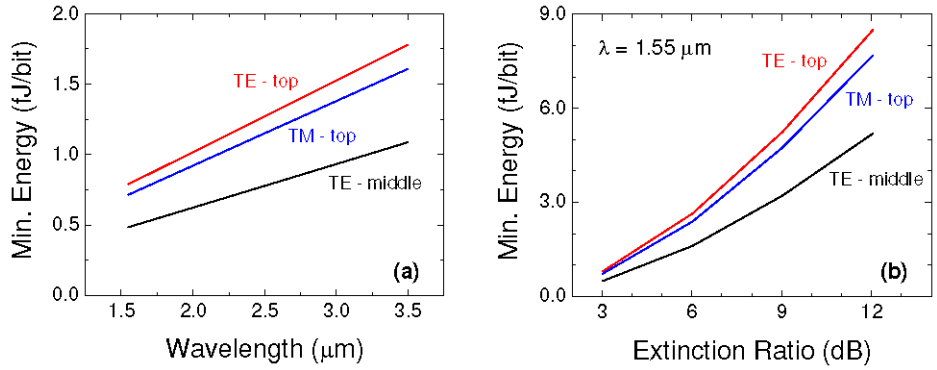

Fig. 4. (a) Plot of minimum energy/bit vs. wavelength for a graphene-on-graphene optical modulator for the three different graphene/waveguide configurations considered in this work. In this plot, *ER* = *L* = 3 dB. (b) Minimum energy/bit vs. extinction ratio, *ER*, at λ = 1.55 μm and *L* = 3 dB.

Finally, we consider the effect of the dielectric layer separating the two graphene sheets on the switching energy. Figure 5(a) shows V_{pp} plotted as a function of the *EOT* value of the dielectric separating the graphene layers for different wavelengths. The figure shows that V_{pp} decreases with increasing wavelength due to the lower quantum capacitance as the Fermi-level is positioned closer to the Dirac point. The reduced quantum capacitance, however, does

#169845 - $15.00 USD Received 13 Jun 2012; revised 11 Aug 2012; accepted 11 Aug 2012; published 20 Aug 2012

not lead to lower energy, since this reduction is exactly compensated by the wider waveguide required at longer wavelengths. The figure shows that even in realistic geometries with *EOT* ~1-2 nm, peak-to-peak voltages less than 0.25 V are still possible. The minimum energy vs. *EOT* for the TE-mode / graphene-on-top modulator geometry is shown in Fig. 5(b). Here, it can be seen that the energy increases at the same rate for all wavelengths, and that in realistic geometries with *EOT* ~1-2 nm, the switching energy is on the order of 2-3 fJ/bit.

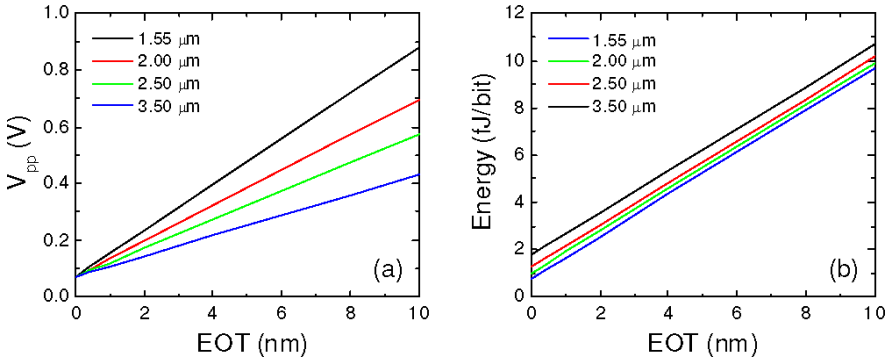

Fig. 5. Plot of (a) peak-to-peak voltage and (b) switching energy per bit vs. equivalent oxide thickness (*EOT*) for graphene-on-graphene optical modulator. For these plots, the graphene is located on the top of a single-TE-mode Si waveguide (Case 2 as described above). In all cases, $ER = L = 3$ dB.

5. Discussion

There are several interesting conclusions that can be drawn from the above analysis. The first is that the energy-per-bit in graphene-on-graphene optical modulators can be very low, at least as low as the best modulators fabricated using Si and SiGe technology. A comparison of the per-bit energy consumption values with other technologies [20–24] is shown in Table II. Here it can be seen that in practical geometries, the minimum energy in graphene-on-graphene modulators is much smaller than Franz-Keldish Effect (FKE) modulators [21,22] and comparable to the more recent Ge/SiGe quantum confined Stark effect (QCSE) results [23,24]. However, the origins of the low-energy consumption, given by Eq. (1), are very different in the different modulator types. In most Si/SiGe modulators, the low energy consumption comes about as a result of the low capacitance of the device, while the operating voltages are still typically around 1 V or even higher. On the other hand, in the graphene-on-graphene modulator, the capacitance is substantially higher, and the low energy consumption is a result of the low operating voltage, which can be as low as 0.1-0.2 V in practical devices, and less than 0.1 V in the ideal limit. This difference is a result of the very different nature of the optical absorption in graphene-on-graphene vs. typical p-i-n diode modulators. In the latter devices, the active region is the i-layer where the optical absorption is modulated, and the p and n regions simply serve as contacts to the i-layer. For efficient modulation, the i-layer must be large enough to overlap or accommodate the optical mode, thus leading to low intrinsic capacitance but requiring relatively-high voltages in order to modulate the field in between. In contrast, in the graphene-on-graphene modulator, the contacts themselves, that is, the two graphene layers, provide the electro-absorption modulation, and the dielectric in between only serves the purpose of preventing current leakage between the two layers. The voltage dropped across the oxide is parasitic in nature, and only serves to increase the applied voltage above the ideal limit. Therefore, for low energy consumption, it is desirable to make this dielectric as thin as possible, increasing the device capacitance, but allowing the device to operate at extremely-low voltages.

#169845 - $15.00 USD Received 13 Jun 2012; revised 11 Aug 2012; accepted 11 Aug 2012; published 20 Aug 2012

Table II. Performance comparison of graphene-on-graphene modulators to literature values for Si/SiGe optical modulators. The graphene modulator parameters were chosen for a single-TE-mode Si waveguide (Case 2) and *EOT* = 1 nm.

Device	V_{pp} (V)	C_m (fF)	*E*/bit (fJ)	*ER* (dB)	Ref.
Si disk	1	12	3	3.2	20
SiGe FKE	3	11	25	8	21
Ge FKE	4	25	100	7.5	22
Ge/SiGe QCSE	1	24	6	5	23
Ge/SiGe QCSE	1	3	0.75	3	24
This work	0.15	289	1.7	3	–

It should be noted that the high capacitance that results when the graphene layers are closely spaced does lead to reduced bandwidth, since no associated reduction in resistance results from the dielectric scaling, and so graphene-on-graphene modulators have a fundamental energy/speed trade-off. Using material parameters (mobility = 4000 cm^2/Vs, and contact resistance = 400 Ω-μm) and RC-limited bandwidth definition reported previously [10], the bandwidth as a function of *EOT* at different wavelengths was calculated and the results are shown in Fig. 6(a). It can be seen that indeed the bandwidth decreases significantly as the graphene layer separation is decreased. The bandwidth is also reduced at longer wavelengths [10], due to the increased modulator area. It should be noted that these bandwidth values are not fundamental and are dependent upon the material parameters, but are shown to provide an estimate of the bandwidth energy trade-offs. Combining the results of Fig. 5(b) and Fig. 6(a), the energy-delay product was calculated and plotted in Fig. 6(b). Here, it can be seen that the energy-delay product is lowest at shorter wavelengths and increases roughly as λ^3, which is a result of the fact that energy-delay scales as $C_m{}^3$, and C_m is proportional to λ.

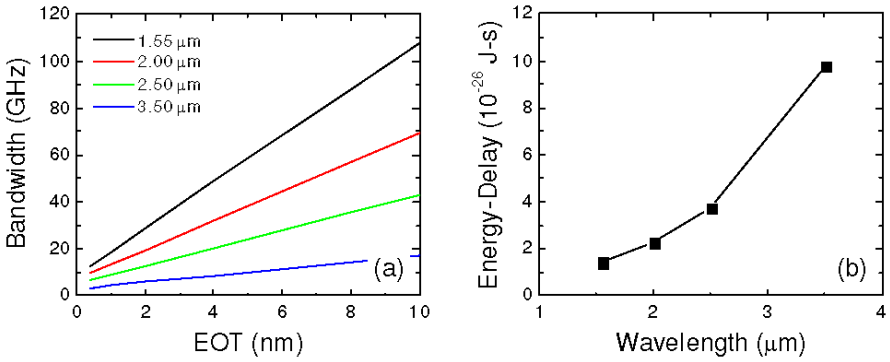

Fig. 6. (a) Plot of bandwidth vs. *EOT* for different wavelengths. (b) Energy-delay product vs. wavelength. Note the results are independent of *EOT*. In both plots, *ER* = *L* = 3 dB.

Despite the trade-offs shown in Fig. 6, the ability to operate at extremely-low voltages could have substantial advantages for low-power optical data transmission, particularly since a trend has been emerging in advanced CMOS technologies that logic devices are operating at ever lower operating voltages. For instance, tunneling field-effect transistors have the potential to reduce supply voltages down to 0.5 or even 0.25 V. In such a case, there could be substantial benefits to having optical interconnects that similarly operate at low voltages, in order to avoid additional power consumption associated with producing multiple power supply domains. The low supply voltage advantage in the graphene-on-graphene modulators can only be realized, however, by precisely doping the graphene layers such that they are tuned to the correct Fermi levels at zero DC bias, which could be a challenging task. The high-capacitance/low-voltage operating mode of the graphene modulators could make the devices much more immune to stray capacitance effects than the low-capacitance/high-voltage devices. This is particularly true when the driver electronics are taken into account,

#169845 - $15.00 USD Received 13 Jun 2012; revised 11 Aug 2012; accepted 11 Aug 2012; published 20 Aug 2012

since these electronics will add substantial additional capacitance to the integrated transceiver elements.

6. Summary

In conclusion, the fundamental switching energy limitations for graphene-on-graphene optical modulators have been described. The minimum switching energy has been calculated to be below 0.5 fJ/bit, under the constraint that the extinction ratio is at least 3 dB, and the insertion loss is no more than 3 dB. The minimum energy was found to increase linearly with wavelength, and the dependence of the switching energy on the wavelength and device dimensions was calculated and the degree to which practical device geometries can approach the minimum energy limit has been described. The results clearly show that graphene-based optical modulators could provide substantial advantages for use in future low-energy optical interconnects.

#169845 - $15.00 USD Received 13 Jun 2012; revised 11 Aug 2012; accepted 11 Aug 2012; published 20 Aug 2012